INHIBITION OF FLAMES BY CONDENSED-PHASE AGENTS

Gregory T. Linteris and Dirk Reinelt,
National Institute of Standards and Technology, Gaithersburg MD 20899, USA

INTRODUCTION AND BACKGROUND

The ban on the production of the fire suppressant CF_3Br has created a need for replacement agents. Obvious alternatives are other halogenated hydrocarbons, and much research has recently been devoted to understanding their relative performance and inhibition mechanisms [1-6]. However, an agent with all of the desirable properties of CF_3Br is proving difficult to find. Consequently, the National Institute of Standards and Technology (NIST) is undertaking research to identify new chemical suppressants and understand the mechanisms of inhibition of known agents, particularly those which have shown strong inhibiting effects.

In the 1960s, Lask and Wagner [7] performed a comprehensive study of the flame inhibiting effects of a wide range of compounds, and determined that organometallic compounds are powerful flame inhibitors. One of the most effective, iron pentacarbonyl $Fe(CO)_5$, a highly flammable, viscous liquid, was found to be several orders of magnitude more effective than the halogens at reducing the burning rate of premixed hydrocarbon-air flames. The authors attempted, in continuing research [8, 9], to understand iron pentacarbonyl's behavior through spectroscopic measurements in low-pressure flames, but the work was discontinued (presumably due to the rapid adoption of CF_3Br). Consequently, the mechanism of inhibition of $Fe(CO)_5$ remains undetermined for premixed flames, and the agent has not been tested in diffusion flames, which are more representative of fires. Although one would never use iron pentacarbonyl to extinguish fires because of its high toxicity, it is so efficient that an understanding of its inhibition mechanism may provide possible avenues for developing new inhibitors.

Iron pentacarbonyl forms condensed-phase particulates [7] upon passing through a flame, and it is unresolved whether its inhibition mechanism is due to gas-phase or heterogeneous effects [8]. Interestingly, other very effective inhibitors also involve a condensed phase. These include agents which form the particulates after passing through the flame; i.e., flame generated particulates, as well as agents which are initially added as a condensed phase. The former category includes other organometallics compounds such as lead tetraethyl and nickel carbonyl and the halometallic compounds $TiCl_4$ and $SnCl_4$ [7]. A new class of fire suppressants, pyrotechnically generated aerosols [10], may work similarly, since these generate particulates through solid-propellant reactions in a flame separate from the fire to be extinguished. The latter category, powders, includes the widely used alkali salt powders $NaHCO_3$ and $KHCO_3$ [11] and other metal salts [12] which can be several times more effective than CF_3Br. Finally, this latter category also includes a new type of suppressant, non-volatile organic precursors [13] which decompose near the flame to release species with strong inhibiting action.

These condensed-phase agents have many similarities, in particular, their strong inhibiting action and the lack of a complete understanding of their modes of inhibition. For example, the relative importance of physical, thermal, and chemical effects have not been clearly discerned for any of the agents, nor have the roles of heterogeneous versus homogeneous chemistry. The approach in this research is to select one condensed-phase inhibitor and study its action, both experimentally and numerically. Many of the experimental and analytical tools developed will then be applicable to other heterogeneous inhibitors. Because $Fe(CO)_5$ is so effective, it was selected first for further study.

Intl. Interflam '96 Conf., 7th Proc. March 26-28, 1996, Cambridge, England. Franks, C.A., Grayson, S., Eds. Interscience Communications Ltd., London, England, 1996.

The approach in the present research is to use simple laboratory burners, both premixed Bunsen-type flames and counterflow diffusion flames, to obtain global, yet fundamental information on the action of iron pentacarbonyl. The burning velocity and extinction strain rate, both of which provide a measure of the overall reaction rate, are determined with addition of iron pentacarbonyl, while varying the stoichiometry, oxygen mole fraction, flame temperature, and flame location as are possible.

These experiments allow control of the chemical environment, the location where the metal-containing species are formed, and the transport of these species to the reaction zone. Ultimately, the research will include detailed numerical calculations including full chemistry, transport, and particulate growth, chemistry, and dynamics. The present paper describes preliminary experimental results. It consists of two major parts: part one deals with premixed flames whereas counterflow diffusion flames are the topic of part two.

PART I: PREMIXED FLAMES

EXPERIMENTAL APPARATUS AND PROCEDURE

The laminar burning velocity is used in the present work as a measure of the inhibition action of iron pentacarbonyl. For the premixed flame burning velocity measurements, a 1.02 cm diameter nozzle burner [14] produces a 1.3 cm tall Bunsen flame. The burner is placed in a square acrylic chimney with no co-flowing gases. The experimental system has been described previously [15]. In the present work, however, the flame height is held constant and no schlieren images are taken of the flame. Since the burner produces schlieren and visible images which are very nearly straight-sided and parallel, the flame area has been found to remain nearly constant if the flame height is held constant.

Fuel, oxygen, nitrogen, argon, and $Fe(CO)_5$ carrier gas flows are measured with digitally-controlled mass flow controllers (Sierra Model 860*) with a claimed precision of 0.2% and accuracy of 1%, which have been calibrated with bubble and dry (American Meter Co. DTM-200A) flow meters so that their accuracy is 1%. The fuel gas is methane (Matheson, 99.97%), and the oxidizer stream consists of argon (Airgas), nitrogen (boil-off from liquid nitrogen) and oxygen (Potomac Air Gas, 99.8%). All gases pass through heat exchangers prior to entering the burner to maintain them at the laboratory temperature of 23°C. Part of the nitrogen stream is diverted, and bubbles through the $Fe(CO)_5$ (Aldrich) in a two-stage saturator in an ice bath. The gas-flow lines which are located after the saturator but before the point of dilution by the bulk of the gas flow are maintained at 39°C to avoid condensation of the $Fe(CO)_5$.

For these experiments, the inhibitor concentration in the premixed gases is increased and the total flow rate reduced as necessary to maintain the desired flame height. Software control of the gas flows allows reduction in the total flow while maintaining constant values of the stoichiometry, oxygen mole fraction, argon/nitrogen ratio in the diluent (to provide temperature control), and $Fe(CO)_5$ mole fraction. The average burning rate for the flame is determined using the total area method assuming a constant value for the flame area. Although measurement of a true one-dimensional, planar, adiabatic burning rate is difficult [16], the relative change in the burning rate can be measured with more confidence. Consequently, the burning rate reduction in the present work is normalized by the uninhibited burning rate.

*Certain trade names and company products are mentioned in the text or identified in an illustration in order to specify adequately the experimental procedure and equipment used. In no case does such identification imply recommendation or endorsement by the National Institute of Standards and Technology, nor does it imply that the products are necessarily the best available for the purpose.

RESULTS AND DISCUSSION

The normalized burning velocity of the premixed methane-air flame inhibited by iron pentacarbonyl is shown in Fig. 1 for a fuel/air equivalence ratio ϕ of 0.9, 1.0, and 1.1. The stoichiometric and rich flames are affected about equally by the $Fe(CO)_5$, while the lean flame shows twice as much reduction in the burning velocity at low $Fe(CO)_5$ concentrations, and could not be stabilized above 24 ppm, where the burning rate reduction is 30%. Most notable, above about 200 ppm, there does not appear to be any additional inhibition effect of the iron pentacarbonyl for the stoichiometric and rich flames.

The flames in Fig. 1 have slightly different adiabatic flame temperatures, calculated using Stanjan III [17] to be 2135, 2227, and 2209 K for ϕ=0.9, 1.0, and 1.1. Hence it is of interest to consider flames in which a constant temperature in maintained while changing ϕ. This is accomplished by replacing nitrogen in the oxidizer stream with argon such that a constant calculated adiabatic flame temperature is achieved, while maintaining the desired stoichiometry and oxygen mole fraction. Figure 2 shows the normalized burning rate of the flames at a constant oxygen mole fraction of 0.21 and a calculated final temperature of 2230 K. As the figure shows, the stoichiometric and lean flames show about the same burning velocity reduction, the lean flame again is hardest to stabilize, and the rich flame shows somewhat less inhibition. Figure 3, in which the equivalence ratio and oxygen mole fraction are constant at 1.1 and 0.21, shows the effect of temperature on these flames. If one extrapolates the highest temperature case to higher $Fe(CO)_5$ mole fractions, it would appear to have the lowest final normalized burning velocity. Hence, as temperature increases, the initial inhibition effect (the slope at low $Fe(CO)_5$ mole fraction) decreases, while the final magnitude of the inhibitory effect increases. The behavior shown in Fig. 1 is a combination of the temperature and stoichiometry effects. The strong inhibition in the lean flame appears to be due to the lower temperature of this flame. The rich flame has a curve similar to the stoichiometric flame because it has a slightly lower temperature, which increases the initial inhibition effect, but has a higher equivalence ratio, which lessens the effect.

The effect of the oxygen mole fraction on the inhibiting effect of iron pentacarbonyl is shown in Figs. 4 to 6, where the normalized burning velocity is plotted as a function of $Fe(CO)_5$ mole fraction. Data are shown for an oxygen mole fraction of 0.20, 0.21, and 0.24 for each of the three values of ϕ (0.9, 1.0, and 1.1) except the case of X_{O_2}=0.20 and ϕ=0.9 where a flame could not be stabilized. As the figures indicate, there is a strong effect of oxygen mole fraction on the initial inhibitory effect, with $Fe(CO)_5$ decreasing the burning velocity about a factor of 3.5 less effectively at an oxygen mole fraction of 0.24 as compared to 0.20. At low oxygen mole fractions (X_{O_2}=0.20 and 0.21), the burning velocity drops rapidly up to an $Fe(CO)_5$ mole fraction of around 100 ppm, and then approaches a constant value for all higher $Fe(CO)_5$ loadings. Conversely, at higher oxygen mole fraction (X_{O_2}=0.24) the decrease in burning velocity is more gradual, but continues to higher $Fe(CO)_5$ loadings, 300 to 500 ppm for these conditions. Also, the final inhibited burning rate is somewhat higher as the oxygen mole fraction increases. An increase in the flame temperature was shown above (in Fig. 3) to similarly reduce the inhibitor effectiveness at low concentrations; however, unlike the higher oxygen mole fraction flames, the higher temperature flames reduce the final burning velocity. Consequently, it is of interest to change the oxygen mole fraction while approximating a constant flame temperature.

Figures 7 and 8 show the normalized burning velocity for a constant calculated adiabatic flame temperature of 2354 K, with oxygen mole fractions ranging from 0.175 to 0.24, for stoichiometric and rich flames. Clearly, there is a strong effect of oxygen mole fraction independent of the

temperature. The inhibitory effect of iron pentacarbonyl at a mole fraction up to 100 ppm is about a factor of four greater at X_{O_2}=0.175 as compared to 0.24. With addition of iron pentacarbonyl above 100 ppm, the low oxygen mole fraction condition shows little incremental inhibition, while the higher oxygen case exhibits a distinctive change in slope, and continues to inhibit the flame up to about 500 ppm.

The variation in iron pentacarbonyl's inhibitory effect with oxygen mole fraction, as well as its variation with X_{O_2} independent of the flame temperature have been determined as a function of $Fe(CO)_5$ concentration. These data supplement the findings of Lask et al. [7] and Bonne et al. [8] which describe a lower effectiveness of $Fe(CO)_5$ with oxygen as the oxidizer rather than air. The next section describes the behavior of iron pentacarbonyl in counterflow diffusion flames, which have a different structure than premixed flames.

PART II: COUNTERFLOW DIFFUSION FLAMES

EXPERIMENTAL APPARATUS AND PROCEDURE

The burner used for the counterflow experiments is described in detail in ref. [18]. It consists of two opposing ducts of 22.2 mm inner diameter which are 11 mm apart. A number of fine wire screens (60 mesh/cm) are placed in each duct to produce laminar flow. Annularly co-flowing nitrogen around the lower duct shields the flame from the ambient air and prevents after-burning of the gases in the exhaust. A water-cooled heat exchanger surrounds the upper duct and mild suction withdraws the combustion products. Because of the high toxicity of iron pentacarbonyl, mild suction is also employed outside the heat exchanger and the experiment is operated in a chemical hood.

The fuel, air, and carrier gas flows are measured with digitally-controlled mass flow controllers described above. The fuel gas methane (Matheson, 99.97%) flows from the top duct, while the oxidizer gas, produced by mixing nitrogen (boil-off) and oxygen (Potomac Air Gas, 99.8%), flows from the bottom. Air could not be used as the carrier gas for the inhibitor due to the reaction of O_2 with $Fe(CO)_5$ and subsequent particulate formation in the bubbler. Therefore, the iron pentacarbonyl is added to the fuel or the oxidizer stream by bubbling methane or nitrogen through a two-stage saturator in a water bath at a controlled temperature of 17-22°C. All experiments were performed at ambient pressure and with the gas flows at ambient temperature.

To run an experiment, a diffusion flame is first established at a predetermined condition of a low strain rate. The strain rate, seen as the maximum value of the oxidizer-side velocity gradient just prior to the flame, can be approximated from the outer flow jet exit velocities according to $a_0 = \frac{2|v_0|}{L}(1 + \frac{|v_F|\sqrt{\rho_F}}{|v_0|\sqrt{\rho_0}})$ [19]. Here L denotes the distance between the ducts, v the velocity, ρ the density and the subscripts F and 0 the fuel and oxidizer stream, respectively. The jet exit velocities are chosen so that the momentum of the two streams is balanced at all values of the strain rate; i.e., $\rho_F v_F^2 = \rho_0 v_0^2$. Doing so ensures that the flame, which is usually close to the stagnation plane, is kept away from the exits of the two gas streams and is found to be approximately in the middle of the ducts. Inserting the momentum balance into the equation for the strain rate gives $a_0 = \frac{4|v_0|}{L}$. If the flame sits on the fuel side of the stagnation plane the equations have to be changed appropriately, leading to $a_F = \sqrt{\frac{\rho_0}{\rho_F}}a_0$, where a_F is the strain rate (i.e., velocity gradient) on the fuel side. When a flame is stabilized the agent is added and the value of the strain rate is gradually increased by proportionately increasing all flows. When the critical value of the strain rate is reached the flame extinguishes abruptly; this value is recorded as the extinction strain rate which is found with an accuracy of ±5%.

NUMERICAL CALCULATIONS

To support the experiments, numerical calculations were made for a gas-phase counterflow diffusion flame. The code was developed by Smooke and is described in numerous publications; e.g., ref. [20]. As a mechanism for methane oxidation, the one-carbon mechanism in ref. [21] is employed. No provision for a condensed phase has yet been made to the code so iron reactions are not included in the calculations. Nevertheless, the calculations are helpful for looking at the uninhibited flames and selecting the conditions for the experiments.

RESULTS AND DISCUSSION

Depending on the dilution of the fuel and the oxidizer stream, the flame will be located on either the fuel or the oxidizer side of the stagnation plane. Additionally, the inhibitor can be added to either the fuel or the oxidizer stream. Hence the inhibitor may be transported to the reaction zone either by convection (fast) or diffusion (slower) after having interacted with an oxidizing or reducing environment. Results for each case are discussed below.

Figure 9 shows the extinction strain rate versus the molar concentration (in ppm) of inhibitor ($Fe(CO)_5$) for the case of undiluted air versus undiluted methane (where the flame is located on the oxidizer side of the stagnation plane). Adding iron pentacarbonyl to the oxidizer stream decreases the extinction strain rate rapidly for mole fractions up to 80 ppm. Above this value, the extinction strain rate decreases less rapidly but roughly in proportion to the increase in $Fe(CO)_5$. Nevertheless, up to the amount of inhibitor used in the experiment (which was limited by the saturator), the incremental inhibiting effect of $Fe(CO)_5$ does not become zero as in the premixed flame.

On the contrary, Fig. 9 shows that adding $Fe(CO)_5$ to the fuel stream increases the extinction strain rate. Iron pentacarbonyl no longer acts as an inhibitor in this case, but rather as a promoter. The increase in the extinction strain rate is small compared to the magnitude of the decrease from addition to the oxidizer stream but it is clearly noticeable. The reason for this increase is unclear. Since thermal decomposition of $1Fe(CO)_5$ may produce $5CO$, tests were conducted to examine the effect of 1000 ppm of CO in the fuel stream when no inhibitor was present. However, both experiments and numerical simulations showed no effect from the added CO.

Contrasting results were obtained with an oxidizer stream of 45% O_2/55% N_2 and a fuel stream of 13% CH_4/87% N_2 (which puts the flame on the fuel side of the stagnation plane). Figure 10 shows the effect of adding $Fe(CO)_5$ to oxidizer and fuel stream, respectively. In both cases, the strain rate at extinction decreases slightly, a few percent at an inhibitor mole fraction of 80 ppm, above which there is no additional effect. Overall, the inhibiting effect of adding iron pentacarbonyl to that flame is almost negligible.

The temperature of the flame on the fuel side, for the conditions of Fig. 10, is much lower than the temperature of the flame on the oxidizer side in Fig. 9. Also, the flame on the fuel side is located closer to the stagnation plane than the flame on the oxidizer side. To eliminate these effects, numerical simulations were run to find a flame on the oxidizer side which is similar to the flame on the fuel side described above. The condition of 30% O_2/70% N_2 versus 20% CH_4/80% N_2 was chosen which gives, according to the calculations, a flame on the oxidizer side which is comparable to the flame on the fuel side with respect to maximum temperature and location of this maximum in relation to the stagnation plane. (It is difficult to determine experimentally the location of the flame relative to the stagnation plane since they are less than 1 mm apart, and the stagnation plane may not be exactly equidistant from the jet exits.)

Figure 11 shows the experimental results of adding $Fe(CO)_5$ to this flame of 30% O_2/70% N_2 versus 20% CH_4/80% N_2. As in Fig. 9, adding iron pentacarbonyl to the oxidizer stream decreases the extinction strain rate. The inhibiting action continues up to 400 ppm and the effect is slightly greater for mole fractions less than 100 ppm. Again, adding the iron pentacarbonyl to the fuel stream leads to an increase of the extinction strain rate. Both effects are not as pronounced as in the case of higher flame temperature of Fig. 9, but the same qualitative behavior is observed. Figures 10 and 11 can be compared more directly since the temperature and distance of the flame from the stagnation plane are comparable; the major difference between them is the location of the flame relative to the stagnation plane. The results show that it cannot be the temperature which plays the most important role but there must be other factors. An important influence is obviously the availability of oxygen for the inhibitor prior to the flame, and possibly different transport rates of the inhibiting species to the reaction zone. It can be seen that the only strong inhibiting effect is performed if the flame is on the oxidizer side and the inhibitor is added to the oxidizer stream.

Since the effectiveness of iron pentacarbonyl in the premixed flames is highly dependent on the oxygen mole fraction, this parameter was also changed in the counterflow diffusion flame. For the case of a flame on the oxidizer side and adding the inhibitor to the oxidizer stream, the oxygen mole fraction was changed while keeping the stoichiometric mixture fraction constant. The stoichiometric mixture fraction is: $Z_{st} = (1 + \frac{\nu_{O_2} M_{O_2} Y_{CH_4,F}}{\nu_{CH_4} M_{CH_4} Y_{O_2,0}})^{-1}$ [22], where ν_i denotes the stoichiometric coefficient of species i, M_i the molecular mass, Y_i the mass fraction and F and 0 the fuel and oxidizer stream, respectively. A constant value of 0.0622 was used for Z_{st}.

Figure 12 shows the normalized extinction strain rate ($a_{ext}/a_{ext,0\%Inhibitor}$) versus the molar concentration of iron pentacarbonyl for three different values of the oxygen mole fraction X_{O_2}. The inhibiting effect for $X_{O_2} = 0.21$ and $X_{O_2} = 0.215$ is almost the same whereas the inhibiting effect is stronger for $X_{O_2} = 0.205$. The results suggest that, as in the premixed flame, the oxygen mole fraction is of importance in the counterflow diffusion flame. To confirm these results more experiments have to be run and a broader range of values for X_{O_2} has to be tested. The experimental difficulty is that counterflow diffusion flames are very sensitive to the oxygen content of the oxidizer stream, so that even uninhibited flames have low extinction strain rates at low values of X_{O_2}. This characteristic of counterflow diffusion flames limits the range that can be used for a variation of X_{O_2}.

SUMMARY

The inhibiting action of iron pentacarbonyl on the burning velocity and extinction strain rate of premixed and diffusion flames of methane, oxygen, nitrogen and argon has been examined systematically. In premixed flames, behavior at low and high iron pentacarbonyl mole fractions is distinctly different: the reduction in burning velocity is very strong for an inhibitor mole fraction up to about 100 ppm, above which there is negligible additional inhibition. In the lower range of iron pentacarbonyl concentrations, richer flames, higher oxygen mole fraction, or higher temperatures reduce the inhibitory effect, while at iron pentacarbonyl mole fractions near 500 ppm, the burning velocity reduction is slightly greater at lower oxygen mole fraction, or higher temperature. Note that the effect of oxygen mole fraction occurs even with a constant flame temperature. In counterflow diffusion flames with the flame on the oxidizer side of the stagnation plane and iron pentacarbonyl added to the oxidizer stream, the inhibitory effect is similar to that in premixed flames, although not as intense. The rate of decrease in extinction strain rate is greatest for iron pentacarbonyl mole fractions below 100 ppm; however, in contrast to the premixed flames, the inhibition effect continues even above 500 ppm. The effect of reduced oxygen mole fraction is similar in the premixed and diffusion flames. Interestingly,

when $Fe(CO)_5$ is added to the fuel stream in the diffusion flame, there is an apparent promotion of the combustion. Finally, when the flame is located on the fuel side, there is a negligible effect of $Fe(CO)_5$ when it is added to either stream. Additional research is planned in order to understand the observed behavior.

ACKNOWLEDGMENTS

The financial support of the Alexander von Humboldt Foundation for one of the authors (DR) is gratefully acknowledged. The authors thank Newton and Arnold Liu for assisting with the software development and the premixed flame experiments. Helpful conversations with D. Trees greatly facilitated the diffusion flame experiments.

REFERENCES

[1] Burgess, D.R.F., Jr., Zachariah, M.R., Tsang, W., Westmoreland, P.R., Halon Replacements: Technology and Science, A.C.S. Symposium Series (A.W. Miziolek, and W. Tsang, Eds.), Washington D.C., 1995, pp. 322-340.

[2] Gann, R.G. (Ed.), National Institute of Standards and Technology, Gaithersburg MD, NIST SP 890, 1995.

[3] Sheinson, R.S., Penner-Hahn, J.E., Indritz, D. Fire Safety Journal 15: 437-450, 1989.

[4] Battin-Leclerc, F., Walravens, B., Côme, G.M., Baronnet, F., Sanogo, O., Delfau, J.L., Vovelle, C., Halon Replacements: Technology and Science, A.C.S. Symposium Series (A.W. Miziolek, and W. Tsang, Eds.), Washington D.C., 1995, pp. 289-303.

[5] Richter, H., Rocteur, P., Vandooren, J., Van Tiggelen, P.J., Halon Replacements: Technology and Science, A.C.S. Symposium Series (A.W. Miziolek, and W. Tsang, Eds.), Washington D.C., 1995, pp. 303-321.

[6] Trees, D., Seshadri, K., Hamins, A., Halon Replacements: Technology and Science, A.C.S. Symposium Series (A.W. Miziolek, and W. Tsang, Eds.), Washington D.C., 1995, pp. 190-203.

[7] Lask, G., Wagner, H.G., Eighth Symposium (International) on Combustion, Williams and Wilkins Co., Baltimore, p. 432, 1962.

[8] Bonne, U., Jost, W., Wagner, H.G., Fire Research Abstracts and Reviews, 4, 6, 1962.

[9] Jost, W., Bonne, U, and Wagner, H.G., Chem. Eng. News, 39, 76, (1961).

[10] Kimmel, E.C., Smith, E.A., Reboulet, J.E., Black, B.H., Sheinson, R.S., and Carpenter, R.L., Halon Options Technical Working Conference, Albuquerque, NM, May 9-11, 1995, p. 499-520.

[11] Rosser, W.A., Inami, S.H., Wise, H., Combust. Flame, 7, 107, (1963).

[12] Vanpee, M and Shirodkar, P., Seventeenth Symposium (International) on Combustion, The Combustion Institute, Pittsburgh, p. 787, 1979.

[13] Bannister, W.W., McCarthy, D.W., Watterson, A., Patronick, J., Floden, J.R., and Tetla, R., Halon Options Technical Working Conference, Albuquerque, NM, May 9-11, 1995, p. 357-367.

[14] Mache, H. and Hebra, A., Sitzungsber. Österreich. Akad. Wiss., Abt. IIa, 150: 157, 1941.

[15] Linteris, G.T. and Truett, L.F., "Inhibition of Premixed Methane-Air Flames by Fluoromethanes", accepted for publication in Combustion and Flame, June 1995.

[16] Andrews, G.E. and Bradley, D., Comb. Flame, 18, 133-153, 1972.

[17] Reynolds, W.J., Stanjan-III Equilibrium Program, Stanford, 1985.

[18] I.K. Puri, K. Seshadri, Combust. Flame 65: 137-150, 1986.

[19] K. Seshadri, F.A. Williams, Int. J. Heat Mass Transfer 21: 251-253, 1978.

[20] M.D. Smooke, I.K. Puri, K. Seshadri, 21st Symposium (Int.) on Combustion, The Co bustion Institute, 1986, pp. 1783-1792.

[21] N. Peters, B. Rogg (Eds.), Reduced Kinetic Mechanisms for Applications in Combusti Systems, Lecture Notes in Physics, m15, Springer-Verlag, 1993.

[22] N. Peters, Prog. En. Comb. Sci. 10: 319-339, 1984.

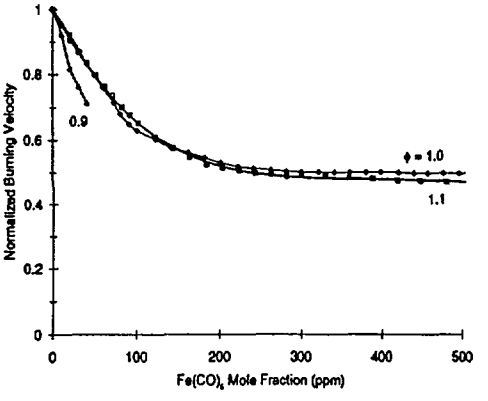

Figure 1: Premixed methane-air flame, X_{O_2}=0.21, ϕ=0.9, 1.0, and 1.1.

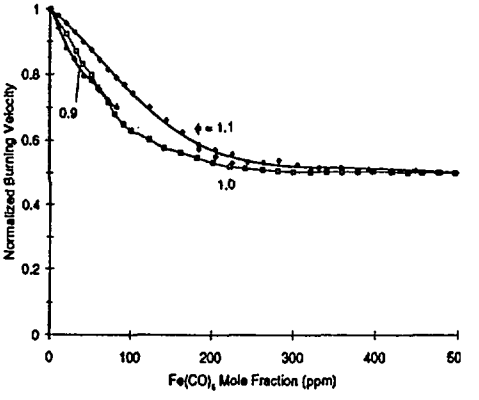

Figure 2: Premixed $CH_4/O_2/N_2/A$ flame, X_{O_2}=0.21, T=2230 K, ϕ=0.9, 1.0 and 1.1.

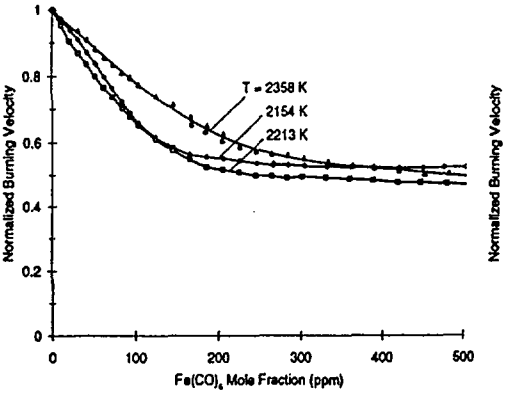

Figure 3: Premixed $CH_4/O_2/N_2/Ar$ flame, X_{O_2}=0.21, ϕ=1.1, T=2154, 2213, and 2358 K.

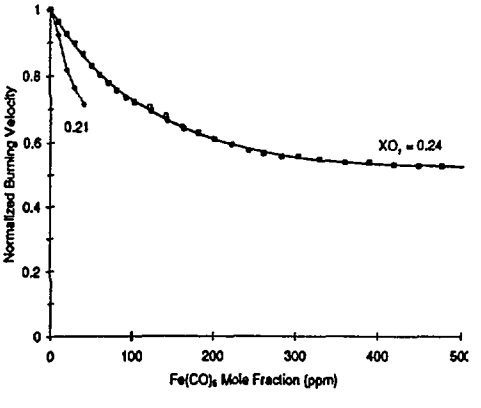

Figure 4: Premixed $CH_4/O_2/N_2/Ar$ flame, ϕ=0.9, X_{O_2}=0.21 and 0.24.

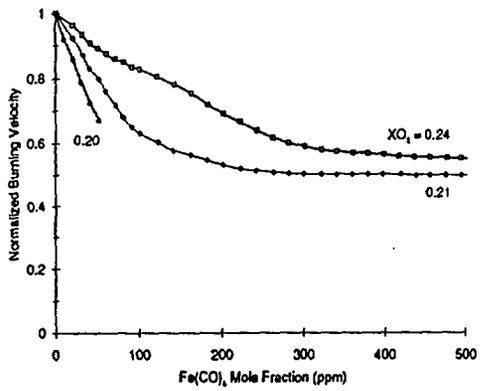

Figure 5: Premixed $CH_4/O_2/N_2/Ar$ flame, ϕ=1.0, X_{O_2}=0.20, 0.21 and 0.24.

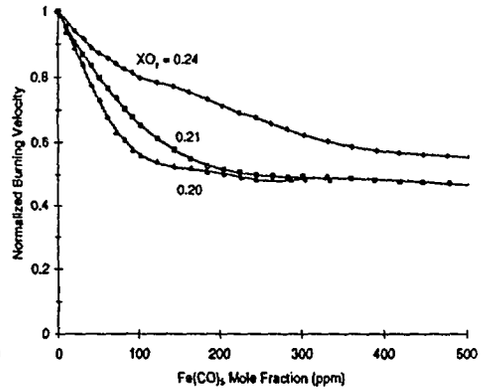

Figure 6: Premixed $CH_4/O_2/N_2/Ar$ flame, ϕ=1.1, X_{O_2}=0.20, 0.21 and 0.24.

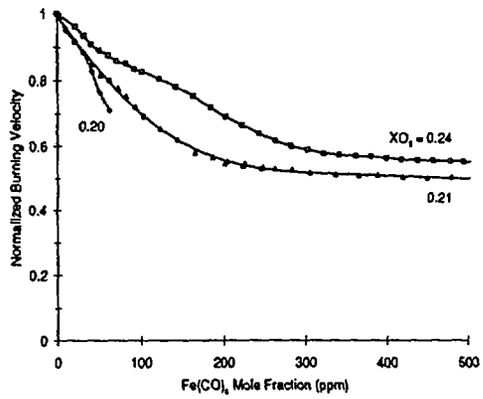

Figure 7: Premixed $CH_4/O_2/N_2/Ar$ flame, ϕ=1.0, T=2354K, X_{O_2}=0.20, 0.21 and 0.24.

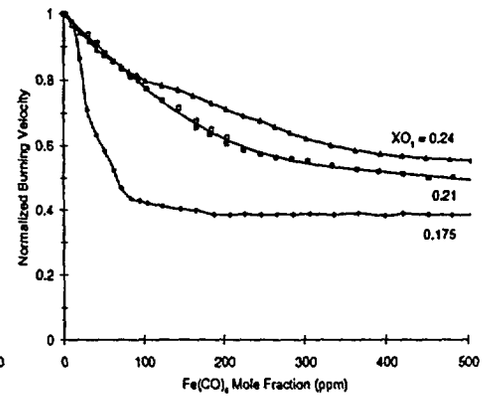

Figure 8: Premixed $CH_4/O_2/N_2/Ar$ flame, ϕ=1.1, T=2354K, X_{O_2}=0.175, 0.21 and 0.24.

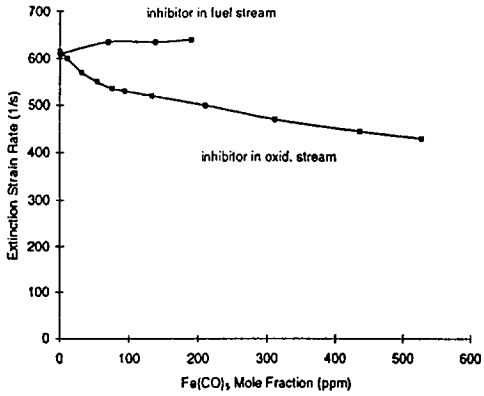

Figure 9: Counterflow diffusion flame; undiluted air versus undiluted methane (flame on oxidizer side).

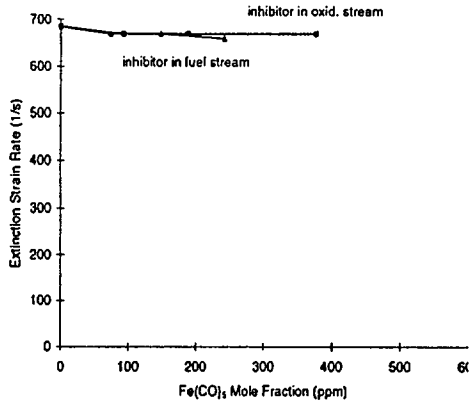

Figure 10: Counterflow diffusion flame 45% O_2/55% N_2 vs. 13% CH_4/87% N_2 (flame on fuel side).

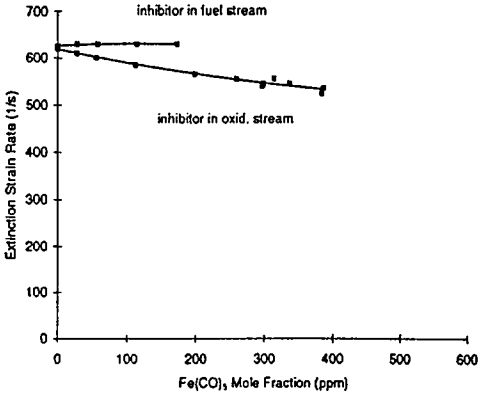

Figure 11: Counterflow diffusion flame; 30% O_2/70% N_2 vs. 20% CH_4/80% N_2 (flame on oxidizer side).

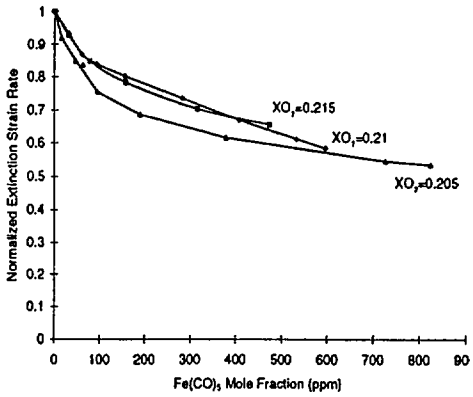

Figure 12: Counterflow diffusion flame; variation of oxygen mole fraction X_{O_2} for constant stoichiometric mixture fraction Z_{st}=0.0622 (flame on oxidizer side, inhibitor in oxidizer stream).